International Meeting on "Best-Estimate" Methods in Nuclear Installation Safety Analysis (BE-2000)
Washington, DC, November, 2000.

BEST-ESTIMATE FACILITY SOURCE TERM ANALYSIS

Martin G. Plys, Boro Malinovic, and Michael Epstein
Fauske & Associates, Inc.
16W070 West 83rd Street, Burr Ridge, IL 60521 USA
Plys@Fauske.com, Malinovic@Fauske.com, and Epstein@Fauske.com

Keywords: source term, multi-compartment facility, combustion, aerosols, fire.

ABSTRACT

Safety analyses of non-reactor fuel cycle facilities and waste facilities often consider handbook look-ups to define bounding source terms for accident scenarios. Here, best-estimate techniques used in reactor safety analysis were applied to create a multiple compartment facility source term analysis program. The program integrates compartment thermal-hydraulics, structural temperature response, fire and combustion sources, aerosol entrainment, and aerosol transport and deposition models, so that the initial source term and the facility leak path factor are explicitly calculated. Examples are provided for blowdown entrainment of fuel particulate, solvent combustion leading to waste entrainment, and propagation of a stratified smoke layer.

1. INTRODUCTION

Safety analysis of non-reactor fuel cycle facilities and waste facilities must consider a broad range of chemical and physical forms of toxic and radioactive compounds, with a broad range of accident initiators and phenomena. An important development in quantification of fuel cycle facility source terms was the compilation of such data in a DOE Handbook (DOE, 1994) usually referred to by the name of its editor, Jofu Mishima, who was also a principal investigator in many release mechanism and release rate studies. While Mishima's handbook contains a detailed information from references, safety analysts often simply pick bounding values recommended in the handbook, motivated by time constraints and to avoid regulatory critique. Removal of conservatism can appear a daunting task because models must usually extrapolate from data and integrate many phenomena.

However, it is common practice in nuclear reactor severe accident analysis to integrate many physical phenomena with best-estimate methods, or at least with methods at the proper level given experimental uncertainty. Therefore, the goal of this work is to extend best-estimate methods for severe reactor accident analysis by incorporating best-estimate source term models for situations pertinent to non-reactor facilities, and apply these methods in lieu of handbook values.

Example computer programs which contain similar facility models are MAAP 4.0 (Henry, Paik, and Plys, 1994; and Schlenger-Faber, et al., 1996) and MELCOR (Gauntt, et al., 1997). Recent example applications of these programs to predict hydrogen distribution in large facilities may be found in (Wolf, Holzbauer, and Cron, 1999) and (Lee, et al., 1999). The computer programs cited above are complex and include detailed models for nuclear reactor primary system and secondary components, but also represent the state-of-the-art for control volume based complex facility models (as opposed to multidimensional flow and heat transfer representations, which are computationally far more complex). This is an appropriate level of sophistication for fuel cycle facility modeling given uncertainties inherent in prediction of chemical reaction and physical entrainment mechanisms for initial release of toxic and radioactive species. However, drawbacks to use of these codes include run time, licensing, user learning curves, relative difficulty in addition of general chemical species not considered in commercial nuclear facilities, and relative difficulty in addition of fuel cycle facility specific source term phenomena.

Our approach to meet modeling needs for non-reactor facilities was to create a general framework similar to MAAP4 and MELCOR, allowing general chemical species through thermodynamic and transport property input, and organized in a modular fashion to incrementally add new phenomena, such as gas phase combustion, fire sources, and various aerosol formation mechanisms. Generic model capabilities are described later in this paper, preceded here first by a brief discussion of model evolution and application.

First use of the method was to examine consequences of hypothetical runaway organic-nitrate reactions in Hanford waste tanks. An experimentally derived reaction rate law was used to define major gas and energy source rates, and this was coupled with a chemical equilibrium calculation of volatile fission product and toxic material release rates. General and tank-specific analyses were performed with the resulting code, ORNATE, but because follow-on efforts in characterization and statistical analysis have shown propagating organic-nitrate reactions to not be credible (Meacham, et al., 1998), no such examples are given here.

Further development has been performed under a Quality Assurance program fully compliant with 10CFR50 Appendix B. Behavior of metallic uranium fuel in multi-canister overpack (MCO) containers was modeled in a computer program named HANSF (HANford Spent Fuel) (Plys, et al., 1999). Its main purpose is evaluation of processing, shipping, and storage of spent nuclear fuel, including exothermic chemical reactions of uranium metal and water release by decomposition of hydrates. An example of particulate entrainment during blowdown is provided here.

Next, we developed a mechanistic model for aerosol release during combustion and post-combustion venting. Its first application was for analysis of hydrogen burns and entrainment of waste from a double-contained receiver tank, or DCRT, leading to the name HADCRT. An example for solvent combustion in a multi-compartment facility, with entrainment of waste, is provided here. Recently, we have extended HADCRT to include fire source models and stratification in compartments, the so-called smoky layer

model in fire analysis. An example of propagation of a combustion product layer between facility compartments completes the work presented here.

2. MODEL DESCRIPTION

HADCRT is a multi-compartment facility model with capabilities similar to MAAP4 and MELCOR cited above, without special models for nuclear reactor primary systems and core melt phenomena, but including models for aerosol formation and entrainment not used for reactor analyses. Compartments in a facility (regions) are individually modeled and connected via an arbitrary network of flow paths (junctions), containing (or joined by) a list of heat conductors. A region may be either well-mixed or stratified and contain a mixture of gases and aerosols.

2.1 Thermodynamics, Heat Transfer, and Intercompartmental Flow

In the well-mixed model, state variables, i.e., conserved quantities, are the mass of each gas m_g, the mass of each aerosol m_a, and the total energy U in each region. The constitutive relation chosen is the most basic non-ideal gas law, the second virial expansion, because this is sufficiently accurate for anticipated conditions. Given mass and energy, temperature T and pressure P in a region are derived auxiliary variables using the non-ideal gas law and the definition total energy as the sum of mass-weighted of specific internal energy u (T, v_g); where $v_g = m_g / V$ is the specific volume, V is the region volume, and the aerosol internal energy is that of the saturated liquid (or solid). So given G substances, there are 2G + 1 conservation equations for the state variables, and 2 auxiliary equations for T and P.

Aerosols are assumed to be in thermal equilibrium with the gas, except when first entrained. When aerosols are in thermal equilibrium, the relative humidity drives either aerosol growth (gas mole fraction exceeds saturation) or evaporation (gas mole fraction below saturation); these rates-of-change are calculated based upon mass transfer correlations. Note the heat capacity of the aerosols is included in calculations, and this is important when substantial material is entrained. Names and physical properties of the species are user-specified and include curve fits for specific heat, second virial coefficient, heat of vaporization, viscosity, thermal conductivity, etc.

Heat transfer and condensation of gases on structures is represented by standard correlations. Within structures the temperature distribution is found by an implicit one-dimensional conduction model allowing layers of varying properties. Conductor surfaces in a region may be joined to form a radiation network, which is important to fire analysis, and can be used for fuel element arrays. Conductors may also be networked to approximate two- or three-dimensional heat transfer.

Intercompartmental flow models account for pressure and density differences between regions; density-driven counter-current flow is discussed more below. A one-dimensional compressible flow model is used for pressure-driven flow and it considers choking, pipe friction, and entrance/exit losses, so that pipe networks can be simulated as well as connected rooms. Aerosols are transported between compartments with the flow.

The model also considers fans, check valves, lifting of covers, one-time failure, and aerosol decontamination by bends and filters. An implicit solution technique is used for stability in the arbitrarily defined network. When the stratified region model is invoked, donor fractions must consider the fraction of each layer passing through a junction.

Except during a combustion event, pressure differences between regions are generally small and density differences cause counter-current exchange of gases between regions. Obviously, a fire source leads to hot, low density combustion gases in a region which is then exchanged in equal volumes with air in an adjacent region. Also, following combustion or sudden release of energy in a region, density differences may persist for a long period. In the long run, counter-current exchanges often provide the driving force for flow from the source location through a facility to the environment. Counter-current flow rates were experimentally determined at Fauske & Associates, Inc. and are discussed in Epstein (1988). Correlations are presented in the reference and include the effect of pressure-driven flow to reduce counter-current flow from its full value when it is purely density-driven, and model validation is not duplicated here.

2.2 Aerosol Agglomeration and Deposition

A key feature of source term analysis is tracking of aerosol agglomeration and setting, which is described here. In most cases of interest, aerosols produced during a single phase of a scenario, and chemical species in the aerosol are well-represented single particle size distribution that evolves with time, and we assume a polydisperse aerosol of uniform composition and time-varying particle size spectrum. Behavior of such an aerosol has been shown by Epstein and Ellison (1988) to obey one of two universal, dimensionless distributions that are independent of the original source characteristics. This source-independence is important because the original source distribution is usually unknown or difficult to quantify.

The reference presents correlations for the sedimentation rate of these distributions under corresponding limiting conditions of: (a) a steady-state source-driven aerosol whose suspended mass is in equilibrium with the source, and (b) a decaying aerosol with negligible source. Correlations are based on exact solution of the integro-differential equation for the aerosol particle size distribution. It is much easier to implement the correlation approach than to implement a sectional aerosol model in a multiple region calculation, with no real loss of accuracy considering uncertainty in input quantities, such as shape factors and true particle densities.

HADCRT calculations are compared against data from Test AB-5 taken at the Containment Systems Test Facility (CSTF), (Hilliard, et al., 1983). CSTF was an 850 m^3 carbon steel vessel, and during Test AB-5, a sodium fire aerosol was pumped in at a rate of about 445 g/s for 900 s, and subsequently allowed to settle for over a day. In Figure 1, it is evident that the aerosol essentially achieves a steady-state during the source period, and about 5 decades in aerosol concentration were experienced during the test. The FAI aerosol correlation used by HADCRT agrees well with data, and is somewhat conservative for the leanest concentrations at the end of the experiment.

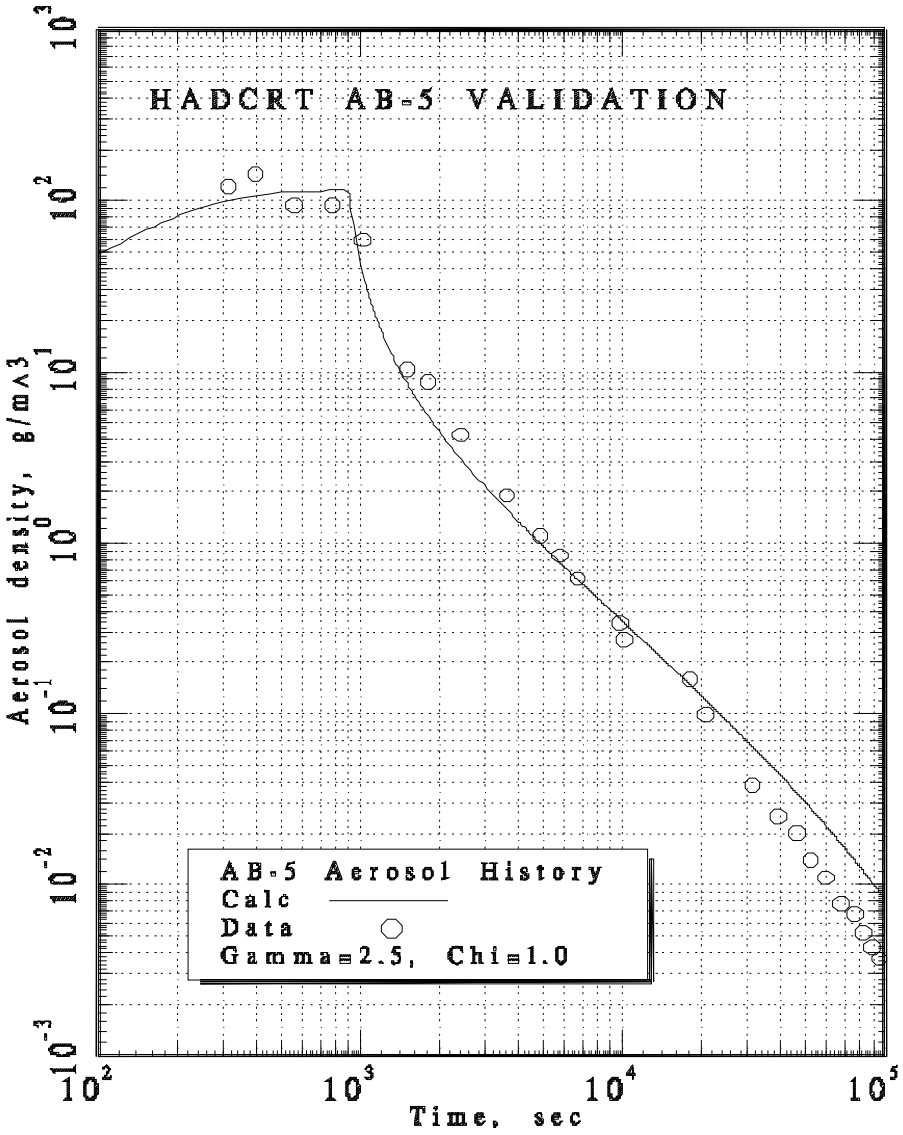

Figure 1: AB-5 Experiment Aerosol Concentration History vs. Calculation.

2.3 Flammable Gas Combustion and Fire Sources

Flammable gas combustion and fire sources are typical events that either directly generate aerosols or lead to entrainment of liquids and particulate. Based upon experience with reactor applications (Plys, 1993), and the fact that initiating events are usually definitions, HADCRT allows the user to specify the burn time for flammable gas combustion rather than perform a flame propagation calculation, as found in MAAP4 and MELCOR. HADCRT allows specification of general solvent vapors containing carbon, hydrogen, and nitrogen for combustion, and can reproduce experimental pressure and temperature histories when a burn time corresponding to appropriate distance and flame speed is used. HADCRT must treat a wide variety of fuels compared to reactor cases, so it is expedient for the user to find literature flame speed data to define the scenario burn time.

Solid and liquid fire sources are also traditionally specified in a scenario, and HADCRT allows fuel burn stoichiometry and rates to be specified in the typical manner. However, a mechanistic model is employed for entrainment of surrounding gases by combustion products which form a plume source to a stratified layer. The well-known Ricou-Spalding (1961) entrainment law is applied in a manner that joins momentum-driven and buoyancy-driven plumes. This is compared against experimental data and theory of Baines and Turner (1969) who injected sources of lower density gas into confined containers of higher density gas and observed plume and stratified layer formation. Figure 2 shows that the position of the stratified layer interface predicted by HADCRT is in accord with the dimensionless representation of data in the reference.

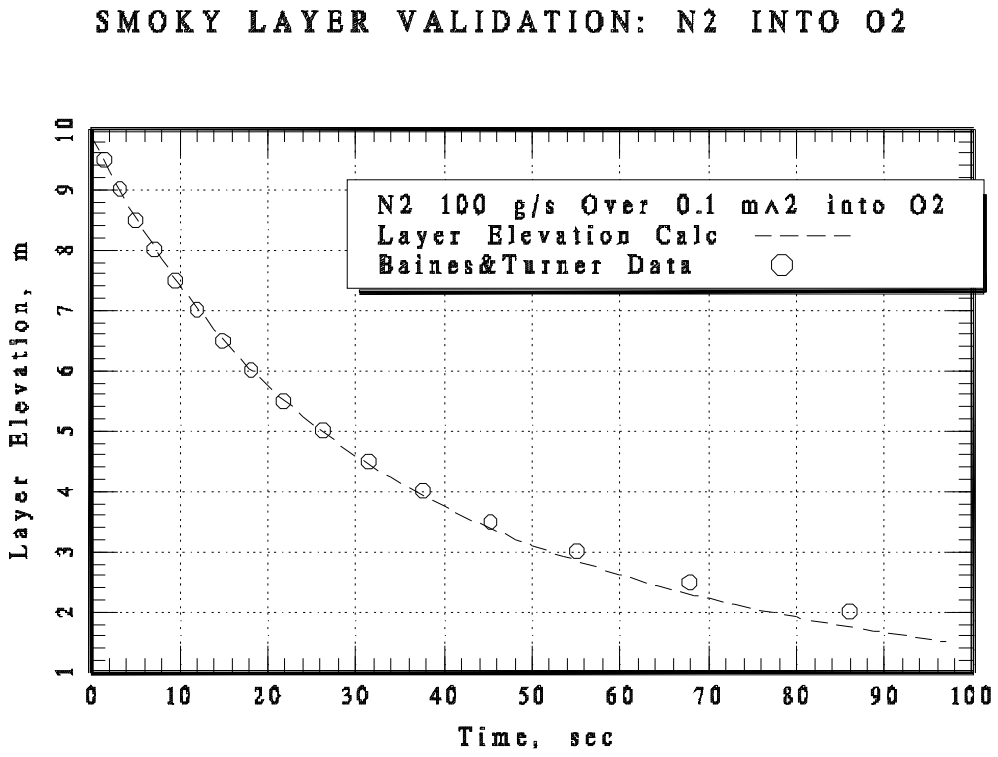

Figure 2: Stratified Layer and Plume Entrainment Validation.

2.4 Aerosol Generation

Aerosol generation mechanisms considered by HADCRT are entrainment of solids from surfaces, stripping of liquid droplets, and direct formation from a fire or user-specified source. The best-estimate approach uses correlations for entrainment and stripping rather than arbitrary source prescription.

Particulate entrainment is based on the correlation of Reynolds and Slinn (1979),

$$\dot{m}''_p = k\,U^3 \qquad (1)$$

where $\dot{m}''_p$ is the entrainment flux, kg/m^2/s, U is the free-stream velocity, and k is the proportionality constant. Reynolds and Slinn quantified the value of k for various conditions, and for smooth surfaces a value between 10^{-5} and 10^{-7} kg s^2/m^5 is appropriate. We are familiar with unpublished work assembled for the Hanford flammable gas program by Gelbard and Brockmann (1997) which substantiates the form of the Reynolds and Slinn law, and which implies that the low end of the parameter is represents most data, and the high end of the parameter can be construed as a bounding value.

An important caveat in use of the entrainment law is that data exist in the range of 1 to 100 m/s, which covers most applications of interest except nearly sonic gas flows and detonations. Detonation speeds are about an order of magnitude larger than the high end of the range of data, and the entrainment correlation is based on the cube of velocity, which leads to large entrainment rates. In application, when a detonation is simulated by HADCRT, enough aerosol is usually created to significantly reduce the pressure and temperature from the otherwise nearly adiabatic values obtained in such short burn durations.

Liquid entrainment is only significant if the free stream velocity exceeds the droplet formation velocity based on the Kutateladze criterion,

$$U_{cr} = 3.1 \left(\sigma g \rho_f / \rho_g^2 \right)^{1/4} \tag{2}$$

where σ is the surface tension, g is the acceleration of gravity, and ρ_f and ρ_g are the fluid and gas densities, respectively. When the critical velocity is exceeded, the Ricou-Spalding entrainment law originally derived for single-phase application is valid for this two-phase application, and yields an entrainment velocity

$$v_e = E_o U \sqrt{\rho_g / \rho_f} \qquad U > U_{cr} \tag{3}$$

where E_o is the Ricou-Spalding coefficient whose value is typically 0.10.

Validation of this approach for two-phase entrainment has been performed by one of us and detailed discussion awaits publication. Stratified flow entrainment was investigated in an air-water system by Yonomoto and Tasaka (1988) who measured quality exiting an opening in the top of a long channel of rectangular cross-section. Airflow through the break entrained liquid droplets, and exit quality increased as the fractional height of stratified water increased from 0.1 to 1.0. The present model is compared with a correlation of results by Yonomoto and Tasaka (1991) in Figure 3.

During combustion, the burn velocity is used for entrainment in the relations above. The gas velocity profile during post-combustion blowdown is described by a potential flow solution:

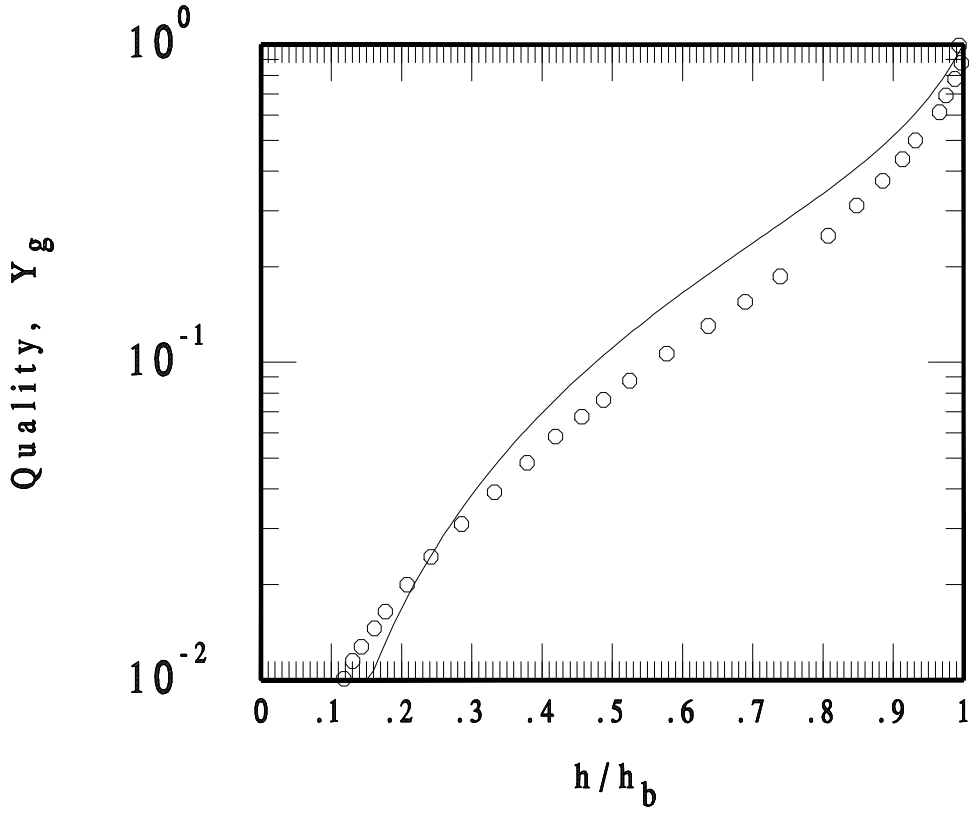

Figure 3: Comparison of Entrainment Model (Solid Curve) With Correlation of Yonomoto and Tasaka Experimental Data (Open Circles) for Liquid Entrainment from a Stratified Region Through a Top Vent.

$$\left|\frac{u\,(x,\,y)}{V}\right| \;=\; \frac{2}{\pi}\sum_{m=1}^{\infty}\frac{\sin\left(\frac{m\,\pi\,b}{R}\right)\sin\left(\frac{m\,\pi\,x}{R}\right)\cosh\left(\frac{m\,\pi\,y}{R}\right)}{m\,\sinh\left(\frac{m\,\pi\,H}{R}\right)} \tag{4}$$

where u is the local horizontal velocity, V is the vent velocity, b is the vent radius, x is the horizontal distance along the tank axis from the vent, y is the vertical distance from the waste surface, R is the maximum distance from the vent to the tank end, and H is the distance from the tank waste surface to the tank top surface. The coordinate system is illustrated as shown in Figure 4. Note, Figure 4 illustrates that the velocity u exceeds the criterion U_{cr} over only a portion of the liquid surface in general. At the centerline and at the tank end (x = R), the horizontal velocity component is so small that no entrainment occurs.

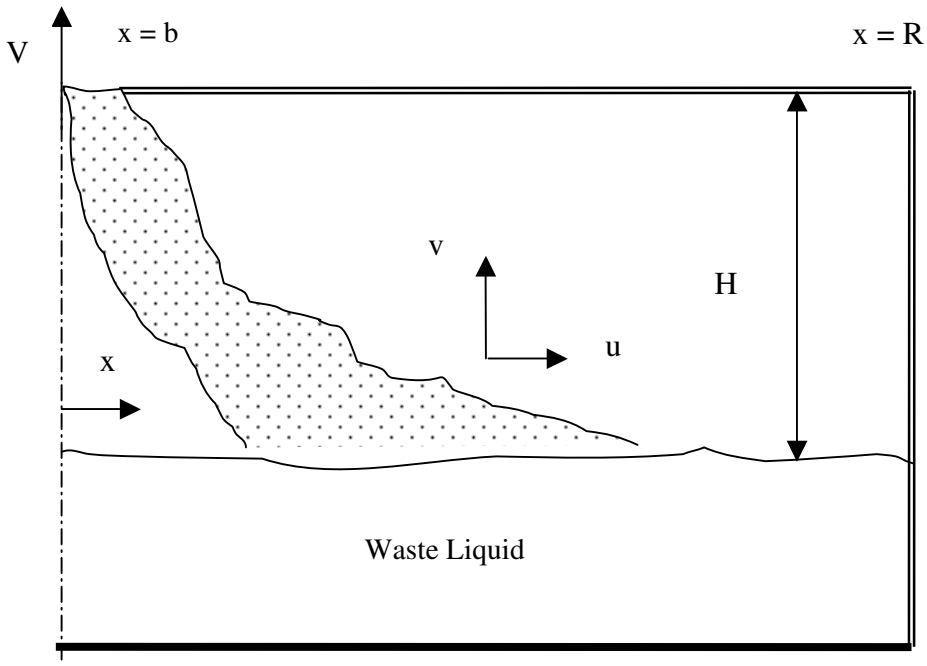

Figure 4: Velocity Profile Solution Coordinate System.

Entrainment from walls is implemented in HADCRT by discretizing the horizontal coordinate x into 20 locations, and discretizing the vertical coordinate into 10 locations. The mesh size was chosen to conform to expected velocity profiles. Each surface area element is assigned a deposited mass in direct proportion to the total material at risk adhering to the wall. At each time step, given the vent velocity V, the velocity at the wall coordinate u (x, y) is used in the Reynolds and Slinn entrainment law to calculate the mass entrainment rate.

2.5 Stratified Layer Thermodynamics and Exchange Flow

When the stratified layer model is invoked, two sets of gases exist in a region. Therefore the equations to be solved are conservation of mass for each gas and aerosol species and conservation of total layer in each layer, i.e., double the number of equations considered for the well-mixed model. The non-ideal gas law and total energy definition are used to relate mass and energy to temperature and pressure for each layer, in conjunction with two joining conditions: the upper layer pressure equals the lower layer pressure minus the static head up to the interface, and the volumes of each layer sum to the total volume. So there are 4G + 2 conservation equations per region, and 4 auxiliary equations and 2 joining equations allow the solution of T_l, T_s, P_l, P_s, V_l, and V_s, where subscripts indicate smoky and lower layers. Note that a separate equation for the time evolution of the layer elevation - which is traditionally presented in smoky layer formulations - is actually redundant. The energy equation solved for each layer is similar to the single equation used for a well-mixed region, but includes a PV work term:

$$\frac{d\,U_i}{dt} = Q_i + \sum W_k\, h_k - P_s\, \frac{d\,V_i}{dt} \qquad (5)$$

where U_i is the total energy of gases and aerosols, Q_i is the total of all heat sources not due to mass addition, the summation term is over all convection flows, and P_s is the layer interface pressure. The value of dV/dt is derived by writing the energy equation for each layer in terms of temperature, finding the total temperature derivative for each layer in terms of time derivatives of mass, temperature, and volume, and using the two joining equations.

Counter-current exchange rates for a stratified system are calculated using the methods described above given average densities on each side of the opening. Exchange flows between layers of each region are determined by relative elevations of the layers and the neutral plane in horizontal flow. Figure 5 shows an example for one set of relative smoky layer and neutral plane elevations. Here there is some pressure-driven flow which reduces the counter-current exchange and causes the neutral plane to shift from its position in the absence of pressure-driven flow. In the example shown, air from the lower layer is exchanged both above and below the neutral plane, while the smoky layer of one region is propagated to the other region depending upon the direction of density difference, which is not necessarily the same as the direction of pressure difference.

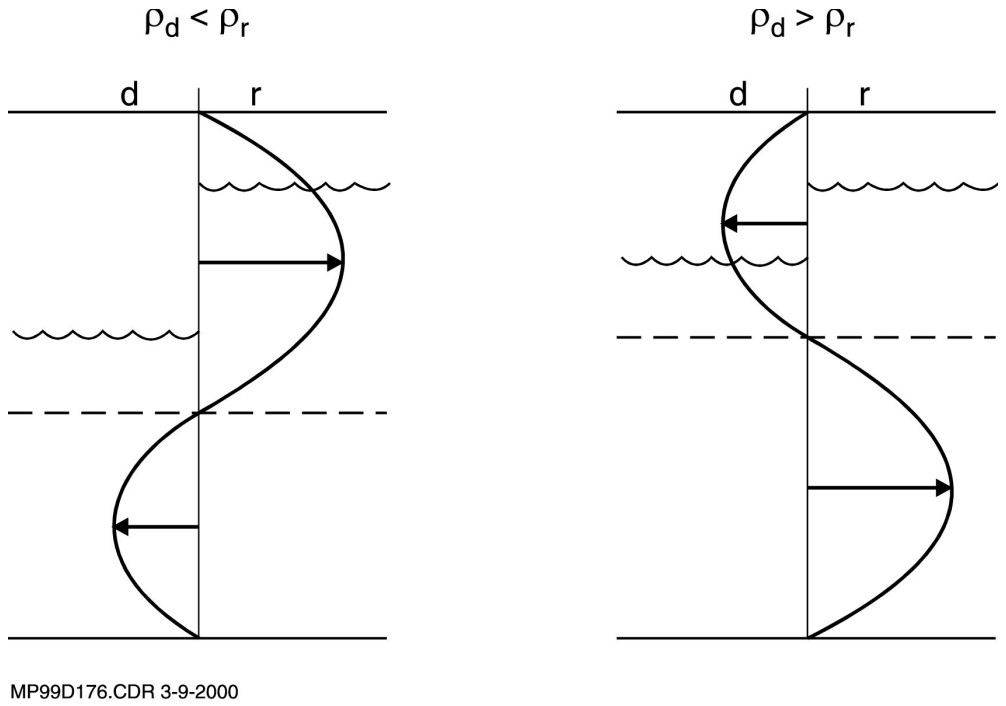

Figure 5: Combined Counter-Current and Pressure-Driven Flows When Higher Pressure (Donor) Region Density Less than Lower Pressure (Receiver) Region Density, Left, and Vice-Versa, Right. Wavy Lines Represent Layer Interfaces, Dashed Line is the Neutral Plane.

3. EXAMPLE CALCULATIONS

3.1 Blowdown Particulate Entrainment

A simple example calculation involves the particle release for multi-canister overpack (MCO) blowdown from high pressure. The MCO design for processing and transporting spent nuclear fuel is a right circular cylinder comprised of stainless steel, with a welded flat bottom, circular head and top "shield plug" containing all penetrations to the MCO interior. An MCO holds five tiers of spent fuel baskets containing either re-racked double annular fuel elements or scrap pieces, as shown in Figure 6. Double annular fuel element assemblies are re-racked into a honeycomb pattern with 54 assemblies per fuel basket, as shown in Figure 7. Damaged fuel is placed in a scrap basket at the top tier. The MCO is 24 inches in diameter, with an overall height of 13'-9.25" and interior free volume of 0.5 m^3. Wall thickness is made ½ inch to withstand extreme pressures, but the MCO is equipped with a ½ inch diameter rupture disk that opens at 150 psig and prevents gross failure.

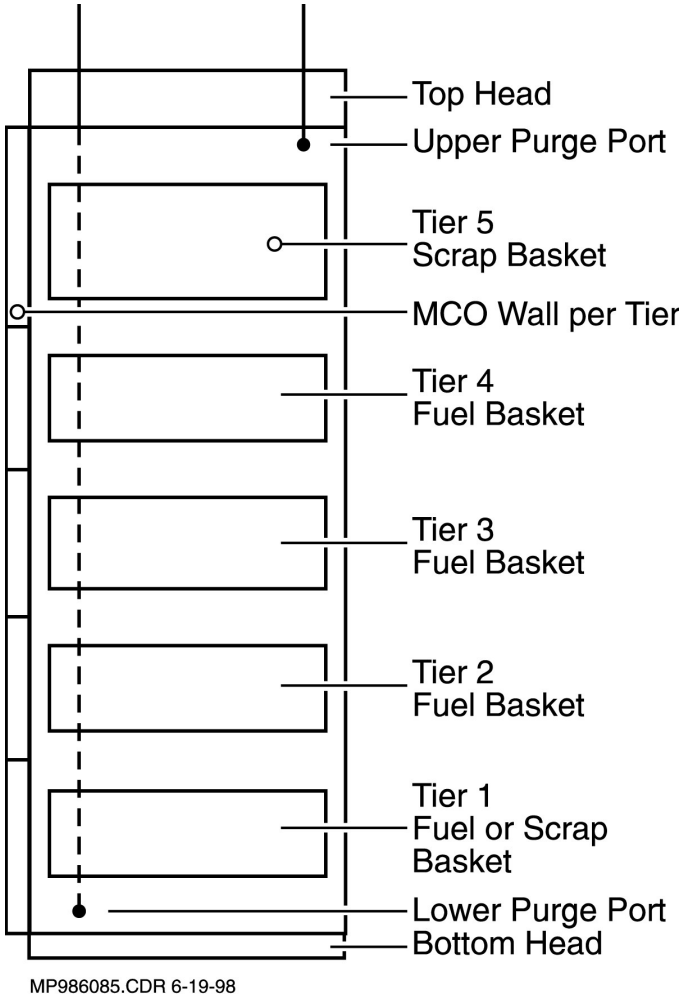

Figure 6: An Multi-Canister Overpack (MCO) Nodalization.

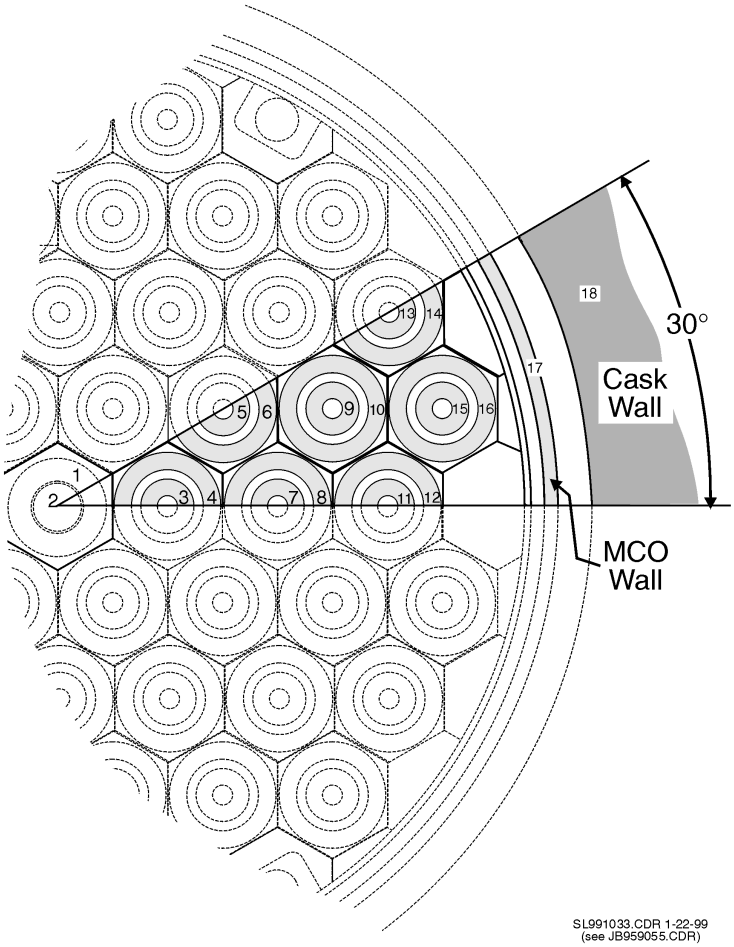

Figure 7: Fuel Basket Cross-Section.

In the presence of liquid water, oxygen, and/or steam, exposed uranium fuel surfaces corrode by taking up oxygen; fuel pieces are clad by and large, but damaged ends and scrap pieces created by transport or handling lead to some exposed surface area available for corrosion. Heat produced by these exothermic reactions is deposited in the fuel and the product, hydrogen, leaves the surface with the fuel temperature. In postulated accident scenarios, the heat of reaction cannot be removed, which causes the hydrogen generation rate to increase exponentially and pressurize the MCO to rupture disk failure. During the subsequent blowdown, gas velocities in the MCO will entrain particulate from fuel surfaces.

The gas velocity profile within the MCO during the blowdown determines the amount of entrainment and the mass of airborne particulate that is ejected to the environment. Assuming that the MCO is at 150 psig initially, the exiting flow is choked and constant for most of the blowdown duration. For initial pressure and temperature conditions of 1.13 MPa (150 psig) and 75°C, respectively, the hydrogen density is 0.78 kg/m^3 and the ratio of specific heats is 1.4. For a loss coefficient of 1.33, the choked flow velocity is found to 714 m/s by using the standard relationships. An estimate of free stream velocity within the MCO is then given by

$$V_{ref} = \frac{W}{\rho A_f} \quad (6)$$

where W is exiting mass flowrate and A_f is the flow area available in the MCO cross-section, which is 0.144 m^2. The reference velocity is therefore 0.62 m/s. To a good approximation, the velocity profile in the MCO during blowdown is uniform across the MCO cross-section and linear along the length of the MCO; i.e., the axial velocity is zero at the bottom of the MCO and increases, with a maximum value of V_{ref} at the top. HADCRT calculates gas velocity using the two-dimensional potential flow solution as shown in equation (4), but in the limit of high aspect ratio (MCO length to diameter), the potential flow solution approaches the approximate velocity profile just described.

In the MCO, 300 kg of fluffy oxide waste powder are spread uniformly across 60 m^2 of fuel and MCO surface areas, which translates to a loading of 5 kg/m^2. (Since the time this work was first completed, the 300 kg material at risk value has been reduced to 30 kg, but for the purpose here, an exact value is unimportant. A reasonable estimate is that if the loading is decreased by an order of magnitude, the source term is decreased by a corresponding amount.) The 60 m^2 surface area is divided into a 20 x 10 mesh, with 20 locations in the coordinate parallel to the flow direction and 10 locations in the coordinate perpendicular to the flow direction. Mesh spacing is finer near the exit because velocity gradients are largest there. At each of the 200 mesh surface elements, entrainment flux is calculated using equation (1) with the time-dependent local velocity, as predicted by equation (4). Total entrainment rate is just the sum of the 200 local entrainment rates. This aerosol generation is then tracked to determine the amount released to the environment.

The model HADCRT for this problem is simple. There are two regions, the MCO interior volume and the environment, connected by one junction. Initial conditions in the MCO are pure hydrogen at pressure and temperature of 1.136 MPa and 75°C. The environment is a large volume of air at one atmosphere and 26°C. There are two heat sinks: one represents the fuel and the other one is the MCO wall.

HADCRT calculates the transient conditions in the MCO and releases to the environment. Blowdown to atmospheric pressure is complete within about 15 seconds. Gas temperature falls to 53°C after 2 seconds, but at the end of the transient, the temperature recovers to match the heat sinks temperatures. Heat sink temperatures barely change from an initial temperature of 75°C and the presence of heat sinks prevents the gas temperature from dropping to unrealistically low values. Figure 8 shows the aerosol generation and transport from the MCO to the environment. The entrainment rate is roughly constant at just over 1 gm/s during the first ten seconds because flow is choked and the exit velocity is constant. Once the flow is no longer choked, the exit velocity decreases with decreasing MCO pressure, and along with it, the gas velocities in the MCO used to calculate entrainment rate. Airborne aerosol mass is also shown. All told, the blowdown generates 15 gm, with 5 gm retained in the MCO and 10 gms released to the environment.

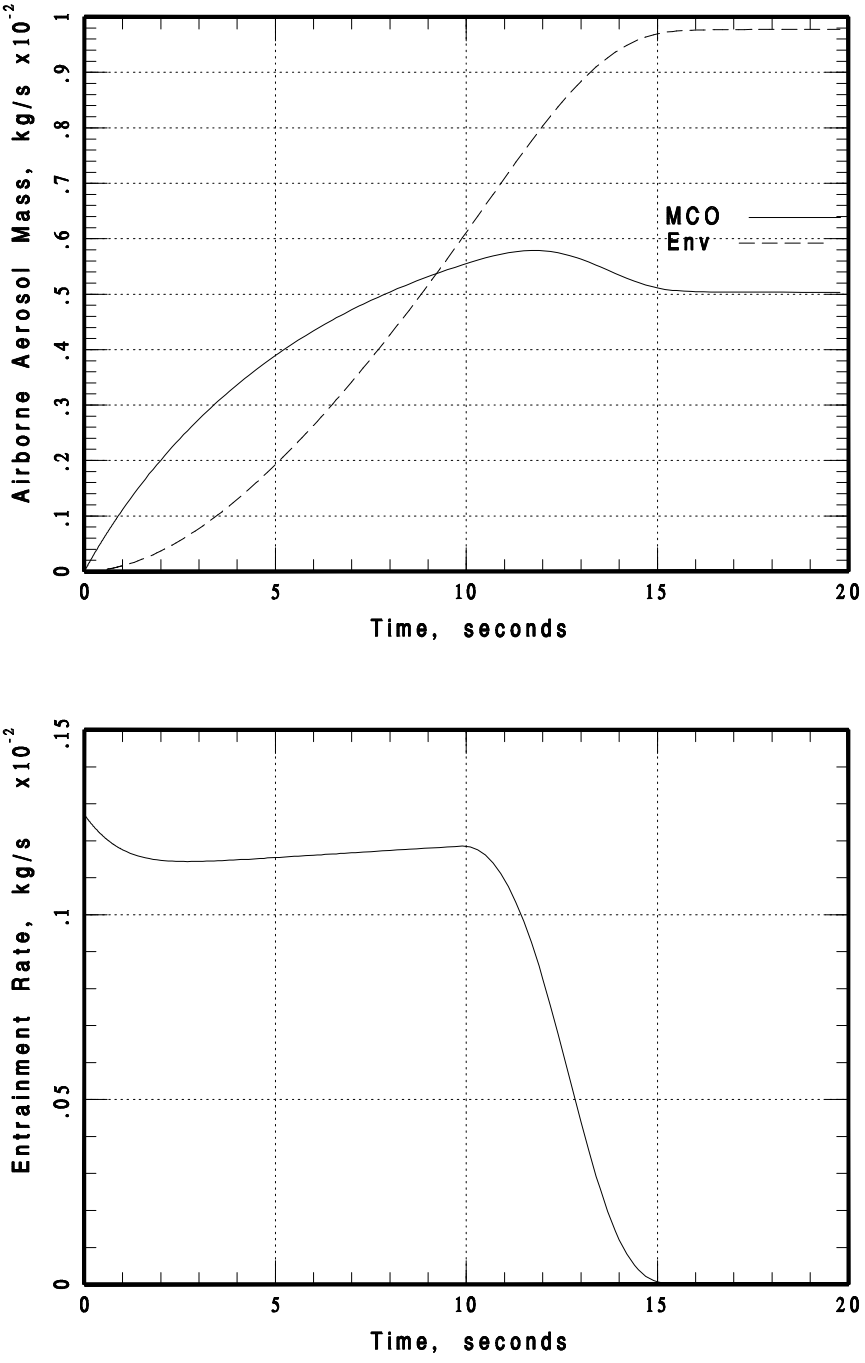

Figure 8: Aerosol Generation and Transport from the MCO to the Environment.

3.2 Solvent Combustion & Waste Entrainment

The example calculation presented here considers a burn in an underground storage tank facility. The facility consists of two underground storage tanks that communicate with each other and with the environment through a system of risers, vents, and manways. Both tanks are nearly empty, save for heels comprised of residual waste

liquids and solids, including hexone solvent. Hexone is a synonym for methyl isobutyl ketone and has the chemical formula $C_6H_{12}O$. The combustion reaction with oxygen is

$$C_6H_{12}O + 8.5O_2 \rightarrow 6CO_2 + 6H_2O \quad (7)$$

Different sources list the lean flammability limit as somewhere between 1.2 and 1.4%. At stoichiometric conditions, hexone, oxygen, and nitrogen concentrations are 2.41%, 20.49%, and 77.10%, respectively. The heat of combustion is then 35.23×10^8 J/kg-mole, or 3.523×10^6 J/g-mole.

The accident scenario postulates that one of the tanks contains a solvent layer at 18°C, so the partial pressure of hexone in the headspace is 1.8%, which is flammable. The initial gas composition is thus 1.8% hexone, 20.62% oxygen, and 77.58% nitrogen. Flammability limit data for compounds similar to hexone show that complete combustion can be expected above 1.6%.

The accident scenario can be described by six steps:

1. Ignition and combustion are assumed to begin in a single tank headspace,
2. The flame front entrains particulate from the tank wall surfaces and liquid droplets from the hexone heel,
3. Heat of reaction and product gas generation pressurize the tank headspace,
4. Combustion ceases and the headspace depressurizes due to flows through the vent lines, risers, and manways,
5. Gas flow inside the tank entrains particulate from the wall surfaces and liquid from the hexone heel, and
6. Gas and aerosols are transported between tanks and the environment.

HADCRT nodalization of the facility is illustrated in Figure 9, which shows four regions, eight junctions (one failure junction and seven normal junctions), and two heat sinks. Regions consist of two underground storage tanks, a filter box, and the environment. Seven normal junctions represent risers to the environment, an open vent line between tanks, an open vent between Tank 1 and the filter fox, and manways that may or may not be bolted shut. Risers are capped shut by flapper valves that will open with only a slight pressure differential. An eighth junction is a failure junction for the weak filter box. The two heat sinks represent the respective tank walls. In the discussion that follows, the nomenclature for the underground storage tank facility stems from the real facility.

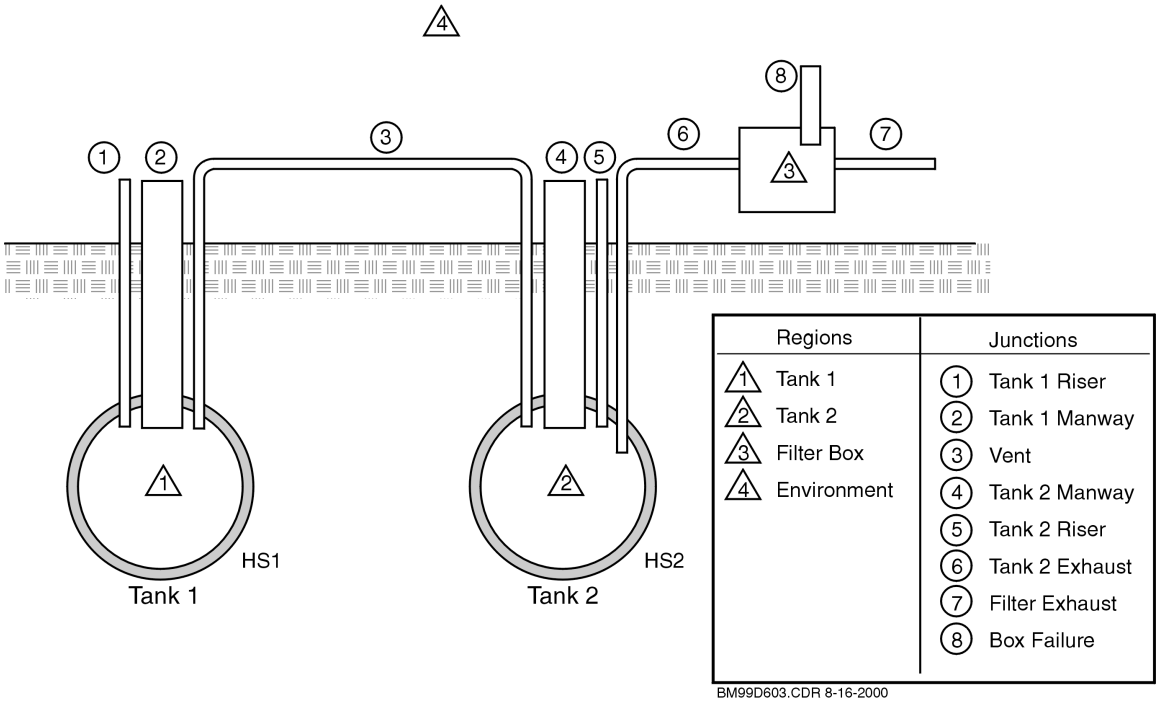

Figure 9: Nodalization for Underground Storage Tank Problem.

The particular case analyzed here has the following characteristics:

- The burn is in Tank 2,
- Manways are bolted shut, and
- Risers are open.

The accident scenario assumes that a burn occurs only in one tank because there is a flame arrestor in the vent line connecting the two tanks. An interesting feature of this facility is that if a burn occurs in only one tank, the other tank acts as a buffer of sorts by providing a relief path and additional volume/deposition area for aerosol settling. In the particular scenario described here, the burn is in the tank near the filter box, although a decontamination factor cannot be credited to the filter box because it has little structural integrity. As Tank 1 pressurizes, exiting flow is split between flowpaths to the environment and the vent to Tank 1. This means that Tank 1 will also pressurize and provide some residence time for aerosols transported from Tank 2.

While combustion and initial blowdown occur within about 2 and 20 seconds, respectively, long-term aerosol release via buoyancy-driven flow occurs for about 30 minutes. Based on AICC calculations, expected values were as follows: peak temperature of a little over 2000 K in Tank 2 and peak pressure just under 0.7 MPa in Tank 2. As shown in Figures 10 and 11, the peak temperature of 2092 K and peak pressure of 0.69 MPa in Tank 2 were attained, and entrained aerosol mass from walls of about 6.5E-4 kg and total release of 1.8E-4 kg at 4 seconds were predicted by the code.

The plots also show pressure and temperature increases in both Tank 1 and the filter box. Because the material at risk was on the order of 100 kg, and a typical handbook release fraction is of order 10^{-3} for this situation, the best-estimate value calculated here is 3 orders of magnitude less than that of the bounding handbook approach.

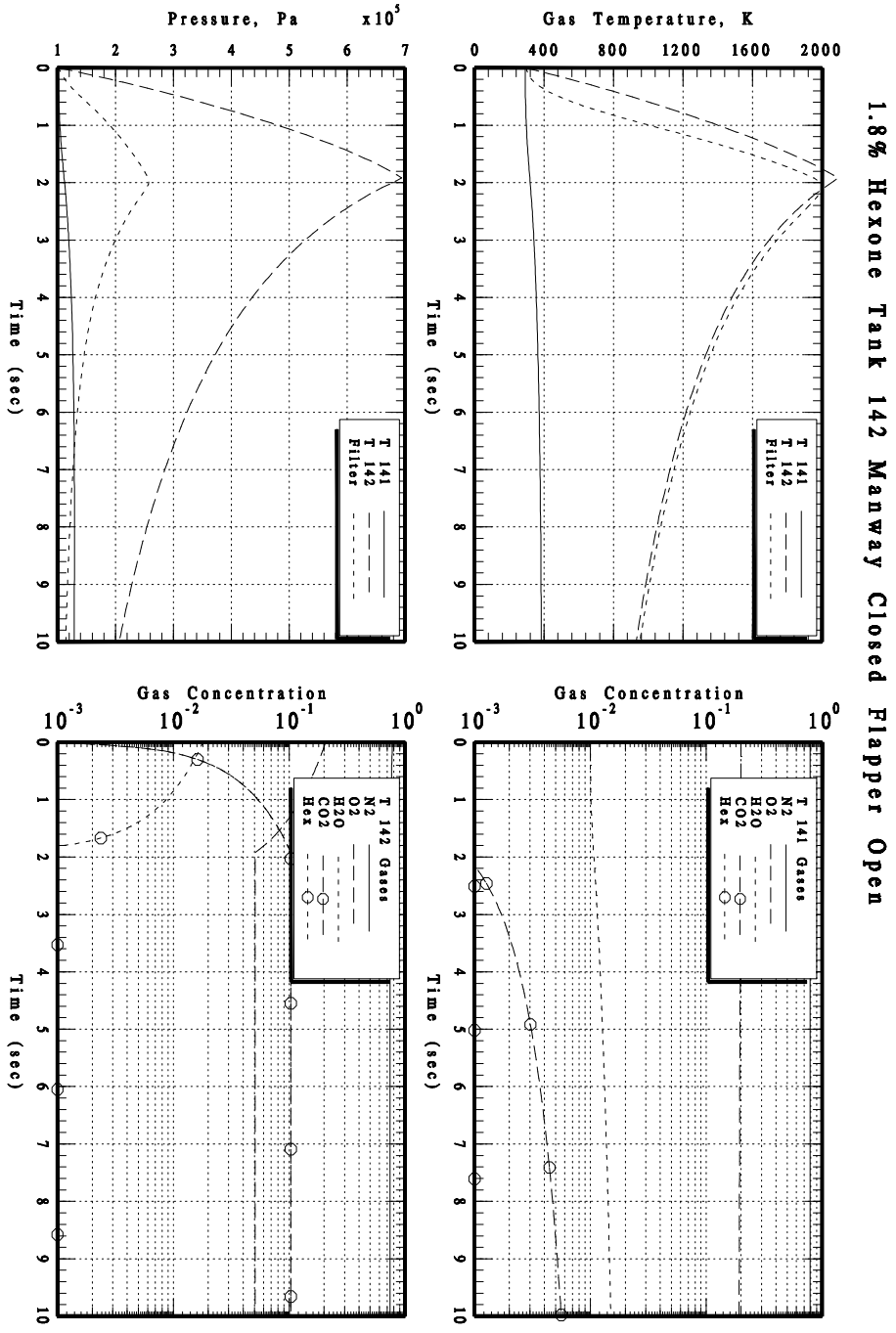

Figure 10: 1.8% Hexone Burn in Tank 2 Pressure, Temperature, and Gas Concentrations.

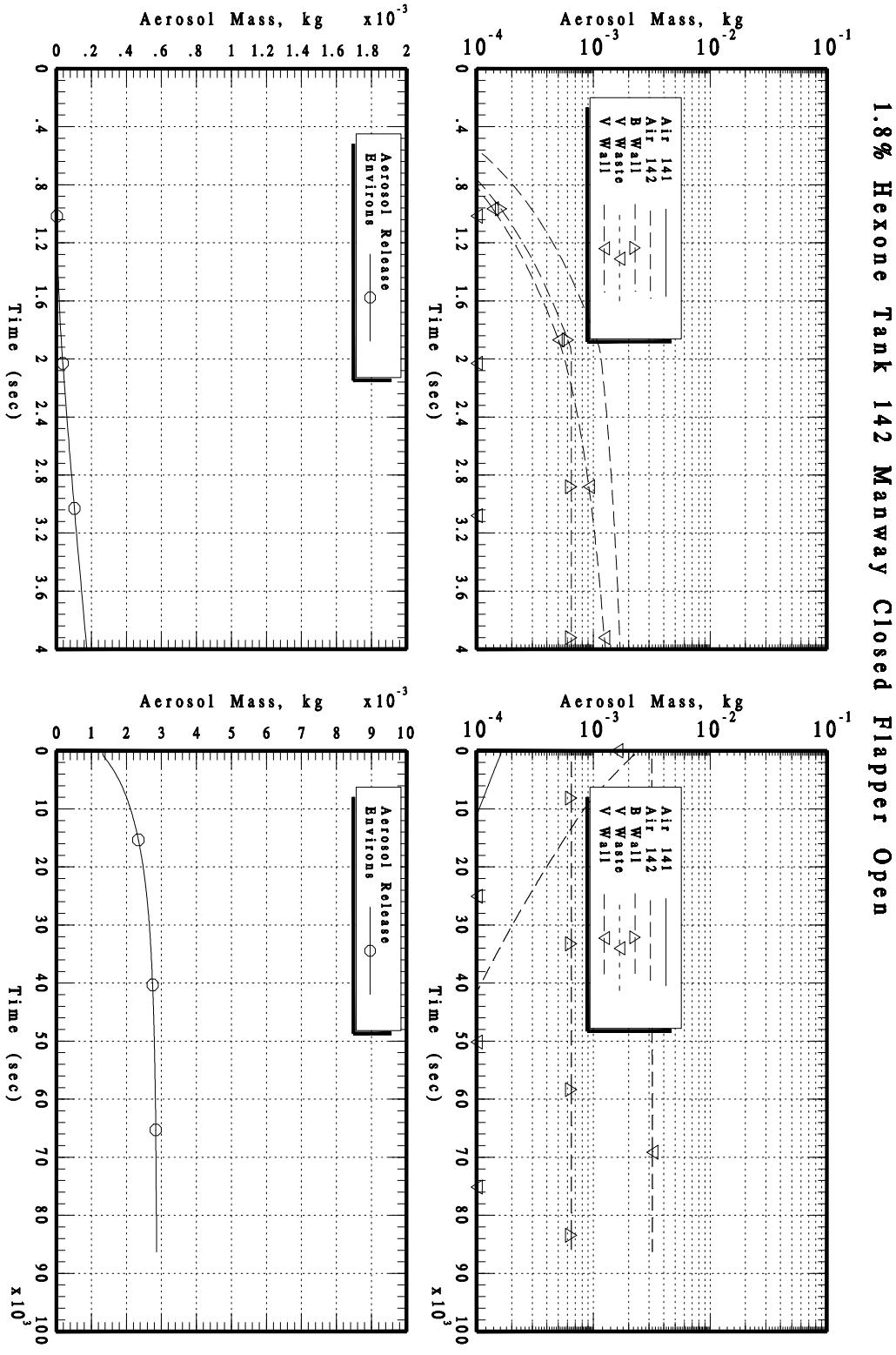

Figure 11: 1.8% Hexone Burn in Tank 2 Entrained Aerosol Masses.

3.3 Stratified Layer Propagation

A simple example of propagation of a stratified layer is given here to illustrate advantages of such a model versus the well-mixed approach. In the example nodalization of Figure 12, four regions are connected via doorways with closed transoms which prevent propagation of a smoky layer until the layer elevation is below the transom, which is at elevation 0.9 m in each doorway. Propagation of a layer initially (and artificially) at 0.5 m in the leftmost region (#1) to the rightmost region (#4) depends on the magnitude of the counter-current exchange rate and the position of the smoky layer relative to the transom. Transient layer elevation histories, Figure 13, verify expected behavior. In contrast, a well-mixed region approach would allow propagation of aerosols from the source room throughout the example regions in just a few time steps. Therefore, the leak path factor for a well-mixed approach will not properly credit attenuation via aerosol sedimentation, and yield overly conservative results compared to a stratified region approach.

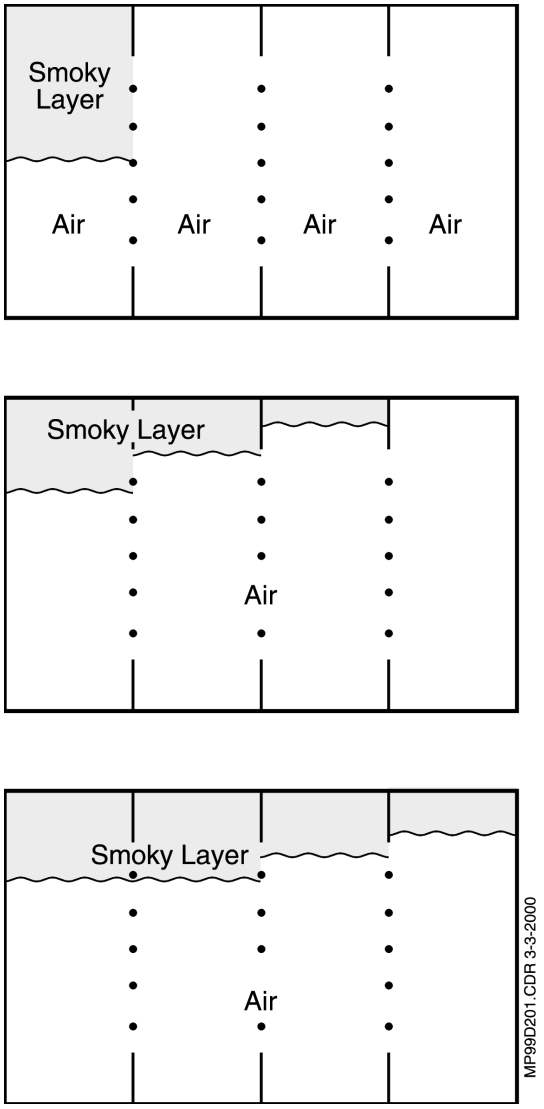

Figure 12: Smoky Layer Propagation Horizontally in a Facility.

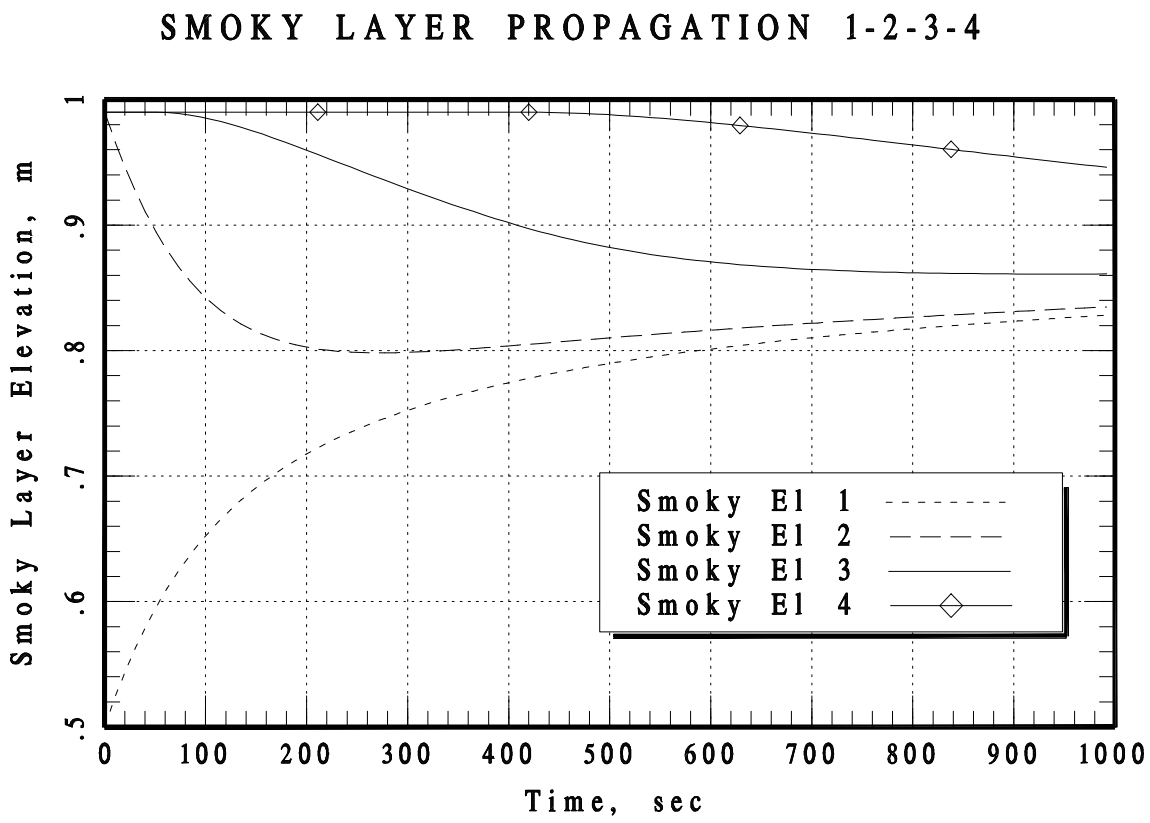

Figure 13: Example of Stratified Smoky Layer Propagation Via Density-Driven Exchange Flow Between Compartments in Series.

4. CLOSING REMARKS

We have shown that methods developed for integrated analysis of reactor accident scenarios can be extended to non-reactor fuel cycle or chemical facility analysis, and we have provided models for commonly encountered scenarios. Though the model framework employs either well-mixed or stratified control volumes, as opposed to a multidimensional solution, the use of correlations and inputs appropriate to points in the control volumes constitutes a best-estimate approach. For example, solid particle entrainment is calculated using local velocities in the Reynolds and Slinn correlation and liquid droplet entrainment is calculated using local velocities in Kutateladze inception criterion and the Ricou and Spalding law.

Separate phenomena models are validated against experimental data to ensure correctness, and to justify the approach as best-estimate. Examples supplied here include aerosol agglomeration and settling, plume entrainment and stratified layer formation, liquid drop entrainment by gas flows over liquid surfaces; and counter-current exchange flows are described in references. User documentation includes a complete set of separate effects comparisons.

We have also shown the combined importance of long-term density-driven counter-current exchange flows in facility analysis. These flows essentially govern the

residence time of aerosols in a facility, and hence, the partition between sedimentation and leakage, i.e., the leak path factor. In this regard, a stratified model approach is preferable for situations in which the released material clearly is not well-mixed in the source region; this distinguishes gas-phase combustion and blowdown entrainment scenarios from fire scenarios for example.

REFERENCES

Baines, W.D., and Turner, J.S., 1969, "Turbulent Buoyant Convection from a Source in a Confined Region," J. Fluid Mech, **37**, Part 1, pp. 51-80.

DOE, 1994, "Airborne Release Fractions/Rates and Respirable Fractions for Nonreactor Nuclear Facilities," DOE-HDBK-3010-94, U.S. Department of Energy, Washington, DC, December.

Epstein, M., 1988, "Buoyancy-Driven Exchange Flow Through Small Openings in Horizontal Partitions," ASME Journal of Heat Transfer, **110**, pp. 885-893, November.

Epstein, M., and Ellison, P.G., 1988, "Correlations of the Rate of Removal of Coagulating and Depositing Aerosols for Application to Nuclear Reactor Safety Problems," Nuclear Engineering and Design, **107**, pp. 327-344.

Gauntt, R.O., et al., 1997, MELCOR Computer Code Manual, NUREG/CR-6119, SAND97-2398, Sandia National Laboratories, Albuquerque, NM, July.

Gelbard, F., and Brockmann, J.E., 1997, "Material Aerosolization", presented at SCOPE Workshop, Hanford Flammable Gas Program, April 30.

Henry, R.E., Paik, C.Y., and Plys, M.G., 1994, "MAAP4 - Modular Accident Analysis Program for LWR Power Plants," Research Project 3131-02, Electric Power Research Institute, Palo Alto, CA.

Hilliard, R.K., McCormack, J.D., and Postma, A.K., 1983, "Results and Code Predictions for ABCOVE Aerosol Code Validation - Test AB5," HEDL-TME 83-16, Hanford Engineering Development Laboratory, November.

Lee, S.J., et al., 1999, "Benchmark of the Heiss Dampf Reaktor E11.2 Containment Hydrogen-Mixing Experiment Using the MAAP4 Code," Nuclear Technology, **125**, pp. 182-196, February.

Meacham, J.E., et al., 1998, "Organic Complexant Topical Report," HNF-3588, DE&S Hanford Inc., Richland, WA, November.

Plys, M.G., 1993, "Hydrogen Production and Consumption in Severe Reactor Accidents: An Integral Accident Perspective," Nuclear Technology, **101**, pp. 400-410, March.

Plys, M.G., et al., 1999, "HANSF 1.3 User's Manual," SNF-3650, Rev. 1, DE&S Hanford, Inc., Richland, WA, March.

Reynolds, B.W., and Slinn, W.G.N., 1979, "Experimental Studies of Resuspension and Weathering of Deposited Aerosol Particles," Oregon State University, Report SR-0980-5 for U.S. DOE, April.

Ricou, F.B., and Spalding, D.B., 1961, "Measurements of Entrainment of Axisymmetrical Turbulent Jets," J. Fluid Mech., **11**, pp. 21-32.

Schlenger-Faber, B.J., et al., 1996, Severe Accident Analysis Using the MAAP Code: Modeling and Applications, Trans. Am. Nucl. Soc., **75**, p. 244.

Wolf, L., Holzbauer, H., and Cron, T., 1999, "Detailed Assessment of the Heiss Dampf Reaktor Hydrogen-Mixing Experiments E11," Nuclear Technology, **125**, pp. 119-135, February.

Yonomoto, T., and Tasaka, K., 1988, "New Theoretical Model for Two-Phase Flow Discharged from Stratified Two-Phase Region Through Small Break," J. Nuclear Sci. and Technology, **25**, pp. 441-455.

Yonomoto, T., and Tasaka, K., 1991, "Liquid and Gas Entrainment to a Small Break Hole from a Stratified Two-Phase Region," Int. J. Multiphase Flow, **17**, pp. 745-765.